19

Study of features in the behavior of optical characteristics of paired nanoparticles taking into account quantum effects

© Yu.A. Eremin, V.V. Lopushenko ¶

Moscow State University, Moscow, Russia

¶e-mail: lopushnk@cs.msu.ru

Received May 08, 2025
Revised July 02, 2025
Accepted July 03, 2025

A comparative analysis of the behavior of optical characteristics of paired silver and sodium nanoparticles with a nanometer gap between them was performed using the discrete sources method. The emerging quantum effects were considered based on mesoscopic boundary conditions using the Feibelman parameters. It was found that the presence of the quantum effect in silver leads to a decrease in the plasmon resonance amplitude and its shift to the short-wavelength region, whereas for sodium particles an increase in the plasmon resonance amplitude and a shift to the long-wavelength region, which can exceed 35 nm, are observed. A study of the field intensity distribution on the particle surface at the plasmon resonance frequency showed that the maxima are achieved at the ends of the particles, and the absolute maximum is located near the gap. At the same time, at distances of about 10 nm along the particle surface, the intensity change can reach 4 orders of magnitude, which is quite significant if we consider that such a distance is only 1.5% of the radiation wavelength in the environment.

Keywords: paired nanoparticles, silver and sodium, quantum effects, mesoscopic boundary conditions, Feibelman parameters, discrete sources method.

DOI: 10.61011/EOS.2025.07.61910.8146-25

Introduction

Nanophotonics is experiencing rapid growth driven by advances in optical physics and emerging nanotechnologies. A key factor is the concentration of light energy into volumes far below the Rayleigh diffraction limit, reaching the nanometer scale [1]. Light localization in ultra-small volumes has been made possible by surface plasmons present in metallic nanostructures. Modern nanotechnologies allow the creation of ultrathin nanostructures, opening prospects for fabricating elements on the order of 1 nm or even smaller [2].

Localized surface plasmonic resonance (SPR) is a fundamental tool for controlling light at the nanoscale. It significantly enhances light-matter interaction on the nanoscale by concentrating the light field into extremely small volumes. In particular, „hot spots“ form in the nanogaps between nanoparticle pairs, where light intensity increases by orders of magnitude. Such structures find wide applications in various technologies, including the manipulation of nanomaterials via optical gradient forces, spectroscopic imaging of single molecules, and plasmonic catalysis for controlling chemical reactions [3–5].

Field enhancement and shifting of SPR position in the frequency domain are achieved by varying the materials of the particle pairs, their sizes and shapes, as well as the gap sizes. Studies of optical properties of particle pairs as a function of their parameters provide valuable information for surface-enhanced Raman spectroscopy (SERS) and achieving significant field enhancement factors, which is highly useful for many biosensing applications [6,7]. The development of innovative biosensors has already led to a considerable expansion of their use in various fields, including medical diagnostics. In clinical practice, they enable early disease detection, especially at low pathogen concentrations, which is critical for timely treatment of cancer and cardiovascular diseases [8].

It should be noted that the optically induced hot spot in the gap between particles critically depends on their structural parameters, material, and gap size, all of which must be selected with high precision. Meeting these requirements is a challenging technological task solved using modern nanofabrication methods, especially when millions of identical structures need to be produced [9,10].

The optical response of plasmonic structures a few nanometers in size can show significant dependence on quantum effects related to the quantum-mechanical nature of the electron gas in plasmonic materials [11]. Non-classical effects become noticeable when the characteristic size of system elements decreases to about 10 nm. At this scale, effects such as spatial nonlocality, electron cloud spillover, and Landau damping begin to play a significant role [12,13].

Calculations performed within time-dependent density-functional theory (TDDFT) are theoretically highly accurate and used in numerous studies. However, their use is limited to metallic clusters up to a few nanometers in size, as the computational complexity of TDDFT grows rapidly with the increasing size of the studied objects, making it impractical for larger systems of real interest [14]. As an effective alternative for accounting key non-classical effects like spatial nonlocality, electron spillover, and Landau damping, an approach using surface response functions (SRF) that

include Feibelman d-parameters is proposed. [15]. This approach greatly simplifies the mathematical description of processes by reducing it to solving classical Maxwell's equations inside the structure with so-called mesoscopic boundary conditions imposed at the surfaces [16].

This work investigates the influence of non-classical effects on near-field optical characteristics of identical dimer pairs consisting of silver (Ag) and sodium (Na) nanoparticles using mesoscopic boundary conditions. The choice of particle materials is motivated by significant differences in plasmon behavior between these metals. For silver, free electrons induced by external excitation spill into the particle volume (spill-in), whereas for sodium, the plasmon extends outside the particle surface (spill-out). [17]. The discrete sources method was used for modeling [18,19]. As established previously, this method provides results for the near field, including inside sub-nanometer gaps, with guaranteed accuracy [20].

Diffraction Problem Statement

We consider the diffraction problem of a P-polarized plane electromagnetic wave $\{\mathbf{E}_0, \mathbf{H}_0\}$ on a pair of axisymmetric, coaxial, homogeneous, identical nanoparticles with smooth boundaries. For simplicity, their combined interior domain is denoted as D_i, and the common boundary as $-\partial D_i \in C^{(2,\beta)}$. The media inside D_i and $D_e = R^3/(\overline{D}_i)$are assumed to be non-magnetic, with dielectric permittivities ε_i and ε_e respectively. Let the plane wave propagate at an angle$\pi - \theta_0$ to the axis of symmetry OZ; then the corresponding field representations can be written as

$$\mathbf{E}_0 = (\mathbf{e}_x \cos\theta_0 + \mathbf{e}_z \sin\theta_0)\chi(x,z), \quad \mathbf{H}_0 = -\sqrt{\varepsilon_e}\mathbf{e}_y\chi(x,z), \tag{1}$$

where $\chi(x,z) = \exp\{-jk_e(x\sin\theta_0 - z\cos\theta_0)\}$, $k_e = k\sqrt{\varepsilon_e}$, $k = 2\pi/\lambda$, $(\mathbf{e}_x, \mathbf{e}_y, \mathbf{e}_z)$ — form the Cartesian basis. The time dependence is chosen as $\exp(j\omega t)$.

With these notations, the diffraction problem with mesoscopic boundary conditions on the scatterer surface can be expressed as:

$$\operatorname{rot}\mathbf{H}_{e,i} = jk\varepsilon_{e,i}\mathbf{E}_{e,i}, \quad \operatorname{rot}\mathbf{E}_{e,i} = -jk\mathbf{H}_{e,i} \text{ in } D_{e,i}, \tag{2}$$

$$\mathbf{n}_i \times (\mathbf{E}_i(P) - \mathbf{E}_e(P) - \mathbf{E}_0(P)) = -d_\perp \mathbf{n}_i \times \nabla\{\mathbf{n}_i \cdot (\mathbf{E}_i(P) - \mathbf{E}_e(P) - \mathbf{E}_0(P))\},$$

$$P \in D_i, \quad \mathbf{n}_i \times (\mathbf{H}_i(P) - \mathbf{H}_e(P)) = \mathbf{n}_i \times \mathbf{H}_0(P), \tag{3}$$

$$\lim_{r\to\infty} r\left(\mathbf{H}_e(M) \times \frac{\mathbf{r}}{r} - \sqrt{\varepsilon_e}\mathbf{E}_e(M)\right) = 0. \tag{4}$$

Here, $\mathbf{r}$ is the position vector of the point $M(x,y,z) \in D_e$, $r = |\mathbf{r}|$, $\mathbf{n}_i$ is the unit external normal to the surfaces ∂D_i and $d_\perp$ is the Feibelman parameter. Note that in boundary conditions (3), a key assumption is that the particle surface ∂D_i represents the metal-dielectric interface; therefore, only one Feibelman parameter appears in (3) [16]. We assume that the solution to the posed problem (2)−(4) is unique.

Discrete Sources Method

The Discrete Sources Method (DSM) is a numerical-analytical surface-oriented method. Within DSM, electromagnetic fields are represented as finite linear combinations of fields generated by low-order multipoles distributed along the common rotation axis of the particles [18]. The constructed approximate solution analytically satisfies both Maxwell's equations inside and outside the scatterers (2) and radiation conditions (4). Unknown amplitudes of the discrete sources (DS) are determined from the mesoscopic boundary conditions (3).

The approximate solution for the case of P-polarization of the external excitation is based on the following vector potentials:

$$\mathbf{A}^{1,\alpha}_{mn} = Y^\alpha_m(\xi, z^\alpha_n)\{\mathbf{e}_\rho \cos[(m+1)\varphi] - \mathbf{e}_\varphi \sin[(m+1)\varphi]\},$$

$$\alpha = i, e,$$

$$A_m n^{2,\alpha} = Y^\alpha_m(\xi, z^\alpha_n)\{\mathbf{e}_\rho \sin[(m+1)\varphi] + \mathbf{e}_\varphi \cos[(m+1)\varphi]\},$$

$$A^{3,\alpha}_n = Y^\alpha_0(\xi, z^\alpha_n)\mathbf{e}_z,$$

where $m = \overline{0, M}$ is the azimuthal harmonic number, $n = \overline{1, N^\alpha_m}$ is the DS index for the m-th harmonic in medium $\alpha = i, e$. Also introduced are the functions:

$$Y^i_m(\xi, z^i_n) = j_m(k_i R_{z^i_n})\left(\frac{\rho}{R_{z^i_n}}\right)^m,$$

$$Y^e_m(\xi, z^e_n) = h^{(2)}_m(k_e R_{z^e_n})\left(\frac{\rho}{R_{z^e_n}}\right)^m,$$

where j_m are spherical Bessel functions, $h^{(2)}_m$ — are spherical Hankel functions satisfying radiation conditions, $k_{i,e} = k\sqrt{\varepsilon_{i,e}}$, $\xi = (\rho, z)$, $\rho^2 = x^2 + y^2$, $R^2_{z_n} = \rho^2 + (z - z_n)^2$, $\{z^\alpha_n\}_{n=1}^{N^\alpha}$ — are DS coordinates, and $(\mathbf{e}_\rho, \mathbf{e}_\varphi, \mathbf{e}_z)$ is the cylindrical coordinate system basis. It is important to note that DS representing the external field $\{\mathbf{E}_e, \mathbf{H}_e\}$ are located strictly within the interior domain D_i.

Using these vector potentials, the solutions to the boundary-value problem (2)-(4) can be written as

$$\mathbf{E}^N_\alpha = \sum_{m=0}^{M}\sum_{n=1}^{N^\alpha_m}\left\{p^\alpha_{mn}\frac{j}{k\varepsilon_\alpha}\operatorname{rot}\operatorname{rot}\mathbf{A}^{1,\alpha}_{mn} + q^\alpha_{mn}\frac{1}{\varepsilon_\alpha}\operatorname{rot}\mathbf{A}^{2,\alpha}_{mn}\right\} + \sum_{n=1}^{N^\alpha_0} r^\alpha_n \frac{j}{k\varepsilon_\alpha}\operatorname{rot}\operatorname{rot}\mathbf{A}^{3,\alpha}_n,$$

$$\mathbf{H}^N_\alpha = \frac{j}{k}\operatorname{rot}\mathbf{E}^N_\alpha, \quad \alpha = i, e. \tag{5}$$

To exploit the axial symmetry of the scatterer, the plane wave field (1) is expanded into a Fourier series over the azimuthal variable φusing the formula

$$\exp\{\pm jx\cos\varphi\} = \sum_{m=0}^{\infty}(2 - \delta_{0m})(\pm j)^m J_m(x)\cos(m\varphi), \tag{6}$$

where J_m is a cylindrical Bessel function and δ_{0m} is the Kronecker symbol. Thanks to axial symmetry of the particle pairs and the solution representation (5) as a finite sum of Fourier harmonics over φ satisfying mesoscopic boundary conditions (3) reduces to sequential stitching of Fourier harmonics of fields on the generating surfaces ∂D_i using a generalized collocation method [21]. Each field harmonic is matched at collocation points distributed on the generating surface of particle rotation, and DS amplitudes $\{p_{mn}^{\alpha}, q_{mn}^{\alpha}, r_n^{\alpha}\}$, $\alpha = i, e$ are determined for individual harmonics numbered m.

The error control of the approximate solution (5) is performed by calculating the surface residuals of the boundary conditions (3) at both collocation points and intermediate points. The plane wave field is chosen as in (1) to eliminate the error in its Fourier series approximation (6).

Numerical Results

We consider a plasmonic structure consisting of a pair of identical metallic elongated nanospherioids with an equivalent volume diameter of $D = 12\,\text{nm}$ and aspect ratio $b/a = 2.5$ each. In this case, the major axis of each spheroid, lying along the axis of symmetry OZ, equals $b = 22.2\,\text{nm}$, while the minor axis size is $a = 8.8\,\text{nm}$. Consequently, the thickness of each spheroid is less than 10 nm. The external excitation, a P-polarized plane wave (1), propagates perpendicular to the symmetry axis of the spheroids, with $\theta_0 = 90^\circ$, and the electric field vector is parallel to the major axis of the spheroids. As previously established, for such excitation, the plasmon resonance amplitude reaches its maximum [20]. The external medium is chosen as free space with a refractive index $n_e = 1.0$ and silicon dioxide SiO_2 with $n_e = 1.46$.

We consider silver (Ag) and sodium (Na) particles, for which Feibelman parameters (FP) are calculated using quantum quantities defined as follows: [22]:

$$\text{Ag: } \hbar\omega_p = 9.17\,\text{eV}, \quad \hbar\gamma = 0.021\,\text{eV},$$

$$v_F = 1.39 \cdot 10^{12}\,\mu\text{m/s}, \quad \mathscr{D} = 9.62 \cdot 10^8\,\mu\text{m}^2/\text{s},$$

$$\text{Na: } \hbar\omega_p = 5.89\,\text{eV}, \quad \hbar\gamma = 0.100\,\text{eV},$$

$$v_F = 1.06 \cdot 10^{12}\,\mu\text{m/s}, \quad \mathscr{D} = 2.67 \cdot 10^8\,\mu\text{m}^2/\text{s},$$

Here, ω_p is the plasma frequency of the metal, γ is the Drude damping rate, v_F is the Fermi velocity, $\mathscr{D}$ is the electron diffusion coefficient, and $\hbar$ is the reduced Planck constant. The frequency-dependent refractive index of silver was taken from a database [23], while the required values for sodium were calculated using the commonly used Drude formula: [15]:

$$\varepsilon_i = 1 - \frac{\omega_p^2}{\omega(\omega - j\gamma)}.$$

In [24] an analytical formula for the FP corresponding to noble metals was obtained as:

$$d_{\perp}(\omega) = -j\,\frac{\varepsilon_i \varepsilon_e}{\varepsilon_i - \varepsilon_e}\,\frac{\sqrt{\beta^2 + \mathscr{D}(\gamma + j\omega)}}{\omega_p \sqrt{\varepsilon_b}}\left(\frac{\varepsilon_b}{\varepsilon_i} - 1\right)^{1.5}, \tag{7}$$

where $\varepsilon_b = \varepsilon_i + \frac{\omega_p^2}{\omega(\omega - j\gamma)}$, $\beta^2 = \frac{3}{5} v_F^2$, v_F — are Fermi velocity parameters. The FP values given by this formula agree well with experimentally obtained data [25]. For sodium particles located in free space, we apply the FP formula:

$$d_{\perp}^0(\omega) = j\,\frac{\xi}{\sqrt{\varepsilon_i}},$$

used for alkali metals [16]. Here, ξ is the spatial nonlocality correlation length in the GNOR model [16], $\xi^2(\omega) = \varepsilon_b \frac{\beta^2 + \mathscr{D}(\gamma + j\omega)}{\omega(\omega - j\gamma)}$. For other external media, the FP is recalculated as:

$$d_{\perp}(\omega) = d_{\perp}^0(\omega)\,\frac{\varepsilon_i + 2\varepsilon_e}{(\varepsilon_i - \varepsilon_e)}\,\frac{(\varepsilon_i - 1)}{\varepsilon_i + 2}, \tag{8}$$

as proposed in [20].

We focus on near fields, specifically, the intensity distribution along the generating surfaces of the nanoparticles at the wavelength corresponding to the plasmon resonance:

$$E(z) = |\mathbf{E}_e^N(z) + \mathbf{E}_0(z)|^2 / |\mathbf{E}_0(z)|^2, \tag{9}$$

where z is the horizontal coordinate along the rotation axis, taking values

$$-b - 0.5\delta \le z \le b + 0.5\delta,$$

with b as the major axis of the spheroid and δ the gap between the spheroids.

We also investigate the frequency dependence of the intensity enhancement factor at the hot spot coordinate $z = 0$, i.e., the center of the gap between the particles.

$$F(\lambda) = |\mathbf{E}_e^N + \mathbf{E}_0|^2 / |\mathbf{E}_0|^2. \tag{10}$$

It is important to additionally note that for silver, the value of $\text{Re}\,d_{\perp}$ calculated by formula (7) is negative, which corresponds to the electron cloud being pushed inside the particle volume (spill-in). However, for sodium, the real part of the Feibelman parameter, as follows from (8), is positive, corresponding to electrons spilling out beyond the metal surface (spill-out).

To obtain quantitative estimates of the influence of quantum effects on the optical characteristics of paired nanoparticles, the graphs below present results obtained both via mesoscopic boundary conditions using surface response functions (srf) and calculations within the classical local response approximation (lra).

In Fig. 1, *a* the dependence of the field enhancement factor in the gap (10) on wavelength is shown for silver and sodium particle pairs in air separated by $\delta = 2\,\text{nm}$. It is clearly seen that for silver pairs, the classical approach (lra)

predicts a plasmon resonance (PR) amplitude exceeding that obtained by the mesoscopic theory (srf); that is, accounting for the quantum effect reduces the PR amplitude (damping) and causes a slight blue shift. Conversely, for sodium particles, including the quantum effect (srf) results in an increased PR amplitude (enhancement) and a red shift. Notably, when the gap decreases to $\delta = 1$ nm (Fig. 1, *b*) the PR amplitude for the Na pair increases fourfold, with a shift of 35 nm relative to the classical case (lra).

Figure 2 shows similar results: graphs of field enhancement in the gap for the same particles but embedded in dense SiO_2 medium at gap distances $\delta = 2$ nm (Fig. 2, *a*) and $\delta = 1$ nm (Fig. 2, *b*) respectively. The increased density of the external medium naturally shifts the PR toward longer wavelengths. Here, the PR for Na particles accounting for the quantum effect (srf) is higher than that obtained from the classical approach (lra) across a wide frequency range. Meanwhile, for Ag particles, the PR behavior is similar to the case in air. This anomalous effect for Na has not been previously observed nor reported in the literature. It is also worth noting that the main PR peak for Na lies in the infrared (IR) region, which may be leveraged for practical applications related to biosensors.

Turning to results on the behavior of the field intensity on the particle surfaces, Fig. 3, *a* shows relative intensity (9) versus coordinate z along the rotation axis, computed along the particle surface cross-section $\varphi = 0^\circ$ for pairs of Ag and Na spheroids at the PR wavelength. Particles are separated by $\delta = 2$ nm in air. The plot shows intensity maxima at the spheroid poles, with the absolute maximum near the gap. Interestingly, the field intensity at the gap center ($z = 0$) is about 2–4 times smaller than at the nearest spheroid poles. More pronounced intensity features on the surface are seen in Fig.3, *b*, corresponding to the reduced gap $\delta = 1$ nm. Here, the field intensity at the Na gap center with quantum effects (srf) is three times lower than at the nearest spheroid poles.

Figure 4 displays analogous intensity distribution results along the surfaces of particles in the denser SiO_2, medium. The relative intensity corresponding to the gap $\delta = 2$ nm is shown in Fig. 4, *a*, where, as before, it can be seen that the intensity reaches its maxima at the poles of the spheroids, with the absolute maximum located near the gap. Similar graphs can be seen in Fig. 4, *b*, which corresponds to a gap $\delta = 1$ nm reduced by half.

A notable common feature across all cases associated with the consideration of the intensity of the total field on the surface of spheroids is that regardless of particle material, gap size, or external medium density, the intensity calculated including quantum effects (srf) almost always exceeds that of the classical model (lra). For sodium particles, this is natural since electrons spill out past particle boundaries forming a plasmonic surface layer. However, this effect for silver has not been previously observed or reported. It should be emphasized that the classical and quantum comparisons are made at different wavelengths.

One more important feature of plasmonic fields should be highlighted. In Fig. 4, *b* or Na particles accounting for quantum effects, the intensity increases by 4 orders of magnitude moving 10 nm from the particle center toward the spheroid pole. This distance corresponds to only 1.5% of the radiation wavelength in the surrounding medium.

Let's focus on certain aspects of the numerical implementation of the Discrete Sources Method (DSM). In all considered examples, the selection of DSM parameters was as follows. The number of harmonics M in the solution representation (5) was determined by the relation between the minor axis of the spheroid a, the wavelength λ and the incident angle θ_0 and was $M = 1$; that is, the non-azimuthal harmonic and harmonics with numbers φ were included $m = 0, 1$. The number of discrete sources (DS) coordinates N_m^α for the m-th harmonic in medium $\alpha = i, e$ was chosen identical for all harmonics and media and was approximately half the number of collocation points L. For a single elongated spheroid ($b > a$), aligned along axis OZ and located at the origin, N discrete sources along axis OZ have coordinates

$$z_i = \sqrt{b^2 - a^2}\cos\theta_i,$$

where $\theta_i = \frac{\pi}{2N} + \frac{\pi(i-1)}{N}$, $i = 1, \ldots, N$. The number of collocation points L was chosen based on the ratio between the generating curve length and the wavelength, and for frequency-dependent calculations, based on the shortest wavelength. This value was kept constant over the entire frequency range. Since the number of collocation points was roughly twice the number of DS, the resulting systems of equations were overdetermined. The coordinates of the collocation points on the generating curve of the elongated spheroid ($b > a$) along axis OZ were chosen as

$$\rho_l = a\sin\theta_l, \quad z_l = b\cos\theta_l,$$

$$\theta_l = \frac{\pi}{2L} + \frac{\pi(l-1)}{L}, \; l = 1, \ldots, L.$$

As previously established [26], this choice ensures uniform reduction of the residual on the surface when L increases.

To illustrate calculation details, consider the fundamentally new results shown in Fig. 2, *a, b* for two different gaps $\delta = 1, 2$ nm. When computing the enhancement factor (EF) for Na particles with a gap $\delta = 2$ nm (Fig. 2, *a*) considering quantum effects (srf) at the plasmon resonance (PR) corresponding to the excitation wavelength $\lambda = 905$ nm, the total number of collocation points on the spheroid generatrices was 196, and the number of DS was 120, ensuring a boundary condition residual norm of l_2, with a magnitude of $1.03 \cdot 10^{-4}$ and 3 accurate significant digits for the EF. A similar result for EF for Na particle pairs with a gap $\delta = 1$ nm (Fig. 2, *b*) in PR mode ($\lambda = 945$ nm) was obtained with 264 collocation points and 156 DS. In this case, the residual was $7.0 \cdot 10^{-5}$, also giving 3 accurate significant digits for the EF.

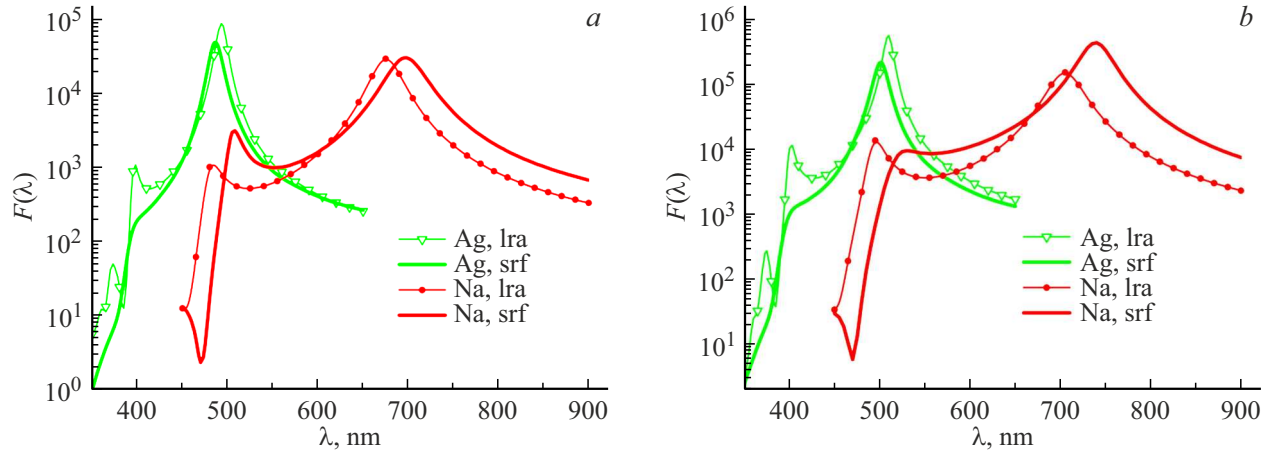

Figure 1. Comparison of the local (lra) and mesoscopic (srf) approaches for pairs of silver and sodium spheroids with various gaps, placed in air, showing the field enhancement factor (10) at the center of the gap: $\delta = 2\,(a)$, 1 nm (b).

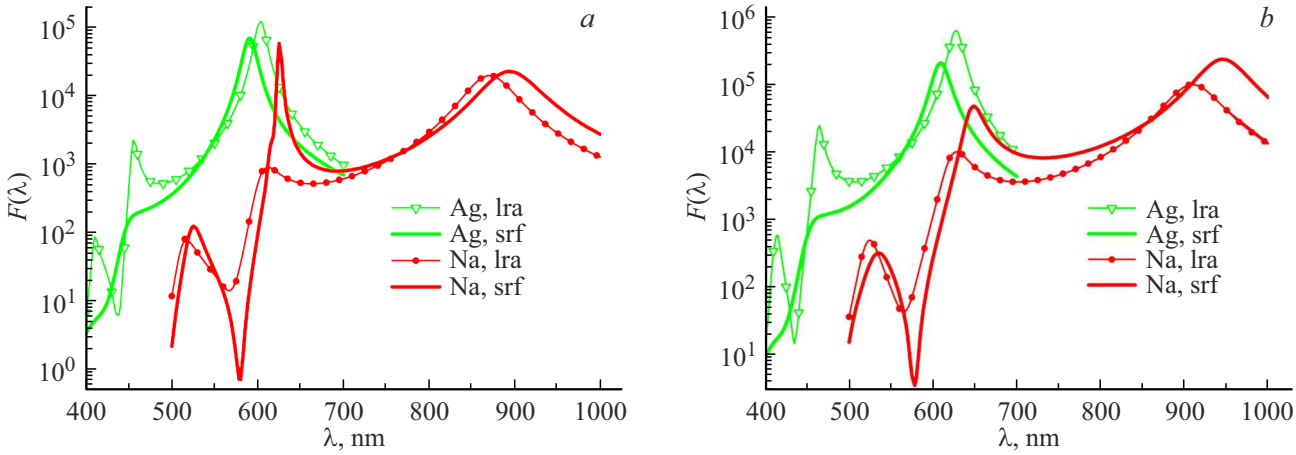

Figure 2. Values of the field enhancement factor (10) in paired silver and sodium particles with different gaps located in a SiO_2 medium: $\delta = 2\ (a)$, 1 nm (b). The results obtained using local (lra) and mesoscopic (srf) approaches are presented.

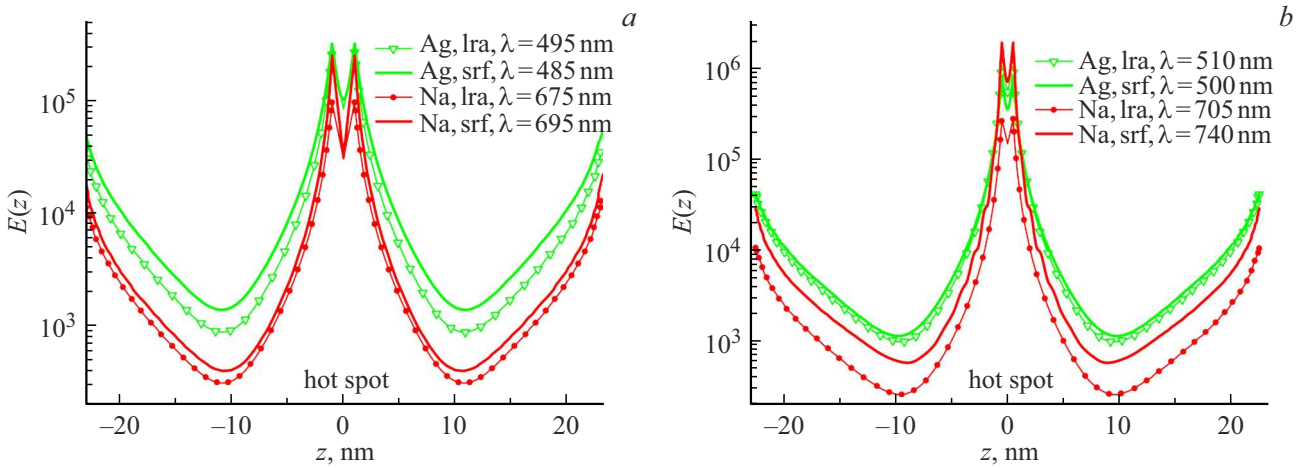

Figure 3. Figure 3 presents the intensity distribution (9) along the spheroid generatrices for local (lra) and mesoscopic (srf) cases, calculated for pairs of silver and sodium spheroids with different gaps in air: $\delta = 2\ (a)$, 1 nm (b).

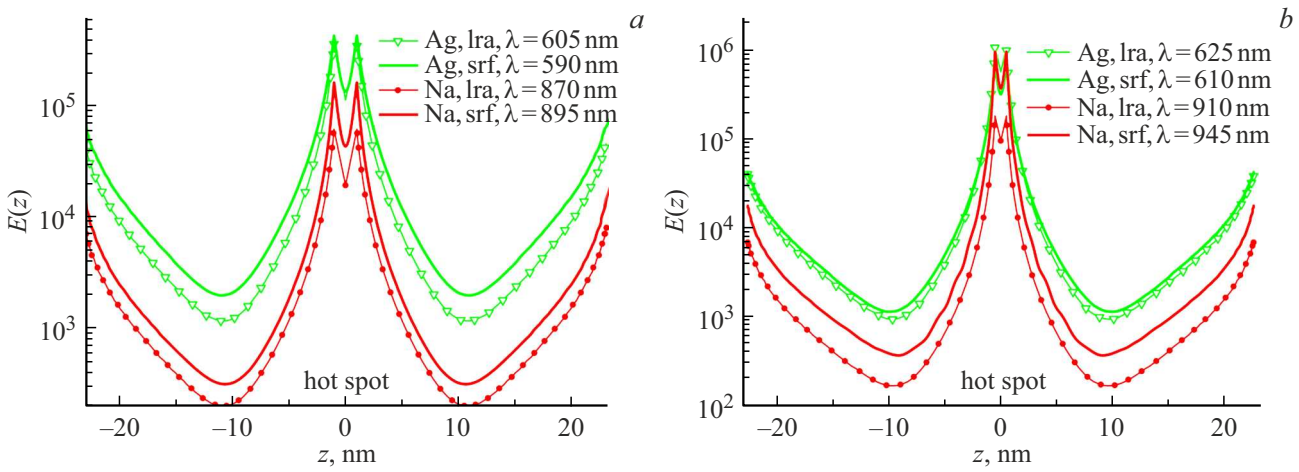

Figure 4. Comparison of the field intensity values (9) along the spheroid generators obtained in the local (lra) and mesoscopic (srf) cases for paired silver and sodium particles located in the SiO_2 medium with different gaps: $\delta = 2$ (*a*), 1 nm (*b*).

Conclusion

The main results of this work are summarized as follows.

Using the DSM, a comparative analysis was performed of optical characteristics of pairs of identical silver and sodium nanoparticles with nanometer gaps between them. The inclusion of arising quantum effects was based on mesoscopic boundary conditions with Feibelman parameters obtained from analytical expressions.

It was established that considering the quantum effect for Ag particle pairs leads to a decrease in the plasmon resonance (PR) amplitude, accompanied by a blue shift of about 5–10 nm, whereas for Na pairs, an increase in PR amplitude is observed, along with a red shift exceeding 35 nm. This result is fundamentally new and has not been previously reported in the literature.

Investigation of the field intensity distribution on the surfaces of spheroidal nanoparticles showed that maxima occur at the spheroid poles, with the absolute maximum located near the gap. Moreover, intensity variation over a 10 nm distance along the particle surface can reach 4 orders of magnitude, an impressive fact considering that such a small distance corresponds to only 1.5% of the wavelength of incident radiation in the surrounding medium. This phenomenon has not been previously noted in the literature.

Funding

The authors' research is supported by the Moscow Center of Fundamental and Applied Mathematics of Lomonosov Moscow State University under agreement No. 075-15-2025-345.

Conflict of interest

The authors declare that they have no conflict of interest.

References

[1] J.W.M. Chon, K. Iniewski. *Nanoplasmonics: Advanced Device Applications* (CRC Press, Boca Raton, 2018). DOI: 10.1201/9781315216423
[2] S.J. Bauman, A.A. Darweesh, M. Furr, M. Magee, C. Argyropoulos, J.B. Herzog. ACS Appl. Mater. Interfaces, **14**, 15541 (2022). DOI: 10.1021/acsami.2c01335
[3] C. Pin, S. Ishida, G. Takahashi, K. Sudo, T. Fukaminato, K. Sasaki. ACS Omega, **3** (5), 4878 (2018). DOI: 10.1021/acsomega.8b00282
[4] T. Yamamoto, H. Yamane, N. Yokoshi, H. Oka, H. Ishihara, Y. Sugawara. ACS Nano, **18** (2), 1724 (2024). DOI: 10.1021/acsnano.3c10924
[5] L. Nan, J. Giráldez-Martínez, A.'Stefancu, L. Zhu, M. Liu, A.O. Govorov, L. VazquezBesteiro, E. Cortés. NanoLett., **23** (7), 2883 (2023). DOI: 10.1021/acs.nanolett.3c00219
[6] Y. Yu, T.H. Xiao, Y.Z. Wu, W.J. Li, Q.G. Zeng, L. Long, Z.Y. Li. Adv. Photonics, **2** (1), 014002 (2020). DOI: 10.1117/1.AP.2.1.014002
[7] C.E. Garrab, M. Zekriti. Physica B: Condensed Matter, **686** (3-4), 416071 (2024). DOI: 10.1016/j.physb.2024.416071
[8] Y. Zheng, X. Song, Z. Fredj, S. Bian, M. Sawan. Anal. Chim. Acta, **1244** (4), 340860 (2023). DOI: 10.1016/j.aca.2023.340860
[9] Q. Pei, X. Zheng, J. Tan, Y. Luo, S. Ye. J. Phys. Chem. Lett., **15** (20), 5390 (2024). DOI: 10.1021/acs.jpclett.4c00964
[10] H.-H. Jeong, M.C. Adams, J.-P. Günther. ACS Nano, **13**, 11453 (2019). DOI: 10.1021/acsnano.9b04938
[11] W. Zhu, R. Esteban, A.G. Borisov, J. Baumberg, P. Nordlander, H. Lezec, J. Aizpurua, K.B. Crozier. Nat. Commun., **7** (1), 11495 (2016). DOI: 10.1038/ncomms11495
[12] C. David, F.J. García de Abajo. J. Phys. Chem. C, **115** (40), 19475 (2011). DOI: 10.1021/jp204261u
[13] C. Tserkezis, W. Yan, W. Hsieh, G. Sun, J.B. Khurgin, M. Wubs, N.A. Mortensen. Int. J. Mod. Phys. B, **31** (24), 1740005 (2017). DOI: 10.1142/S0217979217400057
[14] A. Babaze, E. Ogando, P.E. Stamatopoulou, C. Tserkezis, N.A. Mortensen, J. Aizpurua, A.G. Borisov, R. Esteban. Optics Express, **30** (12), 21159 (2022). DOI: 10.1364/OE.456338

[15] P.E. Stamatopoulou, C. Tserkezis. Optical Materials Express, **12** (5), 1869 (2022). DOI: 10.1364/OME.456407
[16] N.A. Mortensen. Nanophotonics, **10** (10), 2563 (2021). DOI: 10.1515/nanoph-2021-0156
[17] M. Khalid, O. Morandi, Mallet E., P-A. Hervieux, G. Manfredi, A. Moreau, C. Cirací. Phys. Rev. B, **104**, 155435 (2021). DOI: 10.1103/PhysRevB.104.155435
[18] Yu.A. Eremin, A.G. Sveshnikov. Computat. Math. Math. Phys., **61** (4), 564 (2021). DOI: 10.1134/S0965542521040047.
[19] N.V. Grishina, Yu.A. Eremin, A.G. Sveshnikov. Opt. Spectrosc., **113** (4), 440 (2012). DOI: 10.1134/S0030400X12100049.
[20] Yu.A. Eremin, V.V. Lopushenko. Opt. Spectrosc., **131** (8), 1084 (2023). DOI: 10.61011/EOS.2023.08.57294.5402-23.
[21] N.S. Bakhvalov, *Chislennye metody* (Nauka, M., 1975) (in Russian).
[22] S. Raza, S.I. Bozhevolnyi, M. Wubs, N.A. Mortensen. J. Phys.: Condens. Matter., **27**, 183204 (2015). DOI: 10.1088/0953-8984/27/18/183204
[23] P.B. Johnson, R.W. Christy. Phys. Rev. B, **6**, 4370 (1972). DOI: 10.1103/PhysRevB.6.4370
[24] M.H. Eriksen, C. Tserkezis, N.A. Mortensen, J.D. Cox. Nanophotonics, **13** (15), 2751 (2024). DOI: 10.1515/nanoph-2023-0575
[25] A.R. Echarri, P.A.D. Gonçalves, C. Tserkezis, F.J. García de Abajo, N.A. Mortensen, J.D. Cox. Optica, **8** (5), 710 (2021). DOI: 10.1364/OPTICA.412122
[26] Yu.A. Eremin, N.L. Tsitsas, M. Kouroublakis, G. Fikioris. J. Comp. Appl. Math., **417**, 114556 (2023). DOI: 10.1016/j.cam.2022.114556

Translated by J.Savelyeva